Optics Letters

Optical signal acquisition using an alignment robust receiver based on a photodetector array

YUNJIE YAN,[1,2] JORIS VAN KERREBROUCK,[3] NISHANT SINGH,[3] HASAN SALMANIAN,[2]
MING XIANG YANG,[1] YUTONG LIU,[1] ZHENLIN WU,[1] MINGSHAN ZHAO,[1,*] AND
GEERT MORTHIER[2]

[1]*School of Optoelectronic Engineering and Instrumentation Science, Dalian University of Technology, Dalian 116024, China*
[2]*Photonics Research Group, INTEC Department, Ghent University, Technologiepark-Zwijnaarde 126, Ghent 9052, Belgium*
[3]*IDLab, INTEC Department, Ghent University, Technologiepark-Zwijnaarde 126, Ghent9052, Belgium*
*mszhao@dlut.edu.cn

A high-speed receiver module for free-space optical communications with robust alignment, incorporating a previously developed photodetector array (PDA), is presented. The packaged receiver was characterized for the frequency response and transmission performance. By optimizing the PCB on which the array is mounted, a flatter modulation response and higher element bandwidth were achieved. The receiver module exhibited an average 3 dB bandwidth of 2.7 GHz, with an alignment tolerance of 37 µm without mechanical beam tracking. The 3 dB, 6 dB, and 10 dB bandwidth have all significantly improved compared with prior work. In a 25 km SMF transmission demonstration, 10 selected elements operated reliably at 10 Gbps (NRZ). With additional transmitter side equalization, NRZ bit error rates (BERs) below 10^{-12} were achieved at up to 10 Gbps. © 2025

Introduction. With the rapid evolution toward 5G, beyond-5G (B5G) and the forthcoming 6G communication systems [1–3], the demand for ultra-high data rates, low latency, and enhanced connectivity continues to grow. Optical approaches to radio frequency signal extension offer a promising solution to relieve spectrum congestion while supporting the growing demands for higher bandwidth and frequency [4]. Complementary technologies such as visible light communications (VLC) [5], optical wireless communication (OWC) [6,7] and wireless networking with light (LiFi) [8] systems extend optical communication capabilities across diverse deployment scenarios. Free space optics (FSO) systems provide bandwidth advantages and transmission rates comparable to fiber optics [9]. Dense wavelength-division multiplexing (DWDM) implementations have already demonstrated impressive capacities approaching 1 Tbps [10] and the integration of WDM-PAM4 with SLM-based beam tracking in an FSO link achieves a high transmission capacity of 800 Gb/s with a practical 200 m distance [11].

The integration of optical and RF technologies through radio over free space optics (RoFSO) systems represents a particularly promising approach for extending communication capabilities [12]. However, the practical deployment faces substantial engineering challenges, including strict optical alignment requirements, environmental robustness, and complex system integration. A critical bottleneck in RoFSO systems lies in the optical to electrical (O/E) conversion stage. Traditional high-speed photodetectors often exhibit narrow angular acceptance, making the system performance highly sensitive to mechanical vibrations, thermal variations, and optical misalignment. All these factors will result in reduced responsivity, limited bandwidth, and increased bit error rates. While conventional solutions such as microlens arrays [13], beam tracking systems [14], and multicore fiber coupling [15] have been proposed to reduce alignment issues, these approaches typically increase system complexity and cost, while limiting the scalability. Their viability is challenged by efficiency and cost constraints.

In this work, we present an optimized high-speed receiver based on a photodetector array (PDA) designed for robust E/O conversion without mechanical tracking, thereby improving the efficiency of optical signal reception. Data transmission up to 10 Gbps is demonstrated. The receiver provides enhanced alignment robustness of approximately 37 µm compared with conventional approaches, enabled by its large photosensitive area design. The progress represents a significant step towards enabling scalable receivers, paving the way for robust and scalable RoFSO systems.

Design and packaging. The frequency response of the receiver module is limited by the parasitic elements introduced by the packaging, a.o. by the printed circuit board (PCB) on which the InP-InGaAs based PDA is mounted. In this work, we optimized the whole packaging to obtain a better frequency response. In the packaging process, we considered factors such as the PDA chip capacitance, wire bonding, the amount of conductive adhesive, PCB design, and RF connectors.

In the PDA design, the 3 dB bandwidth is primarily determined by the RC capacitance time constant and the carrier travel time, with the latter determined mainly by the absorption
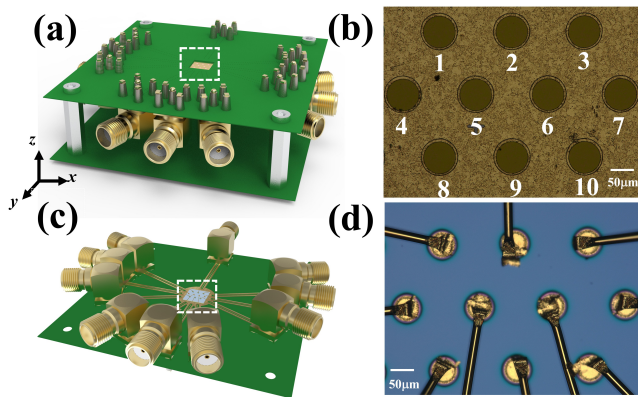
Fig. 1. (a) Schematic of the packaged receiver module. (b) Optical microscope image (top view) of the 10 selected elements employed in the experiment. (c) Bottom view of the receiver module. (d) Optical microscope image (bottom view) of the chip, with gold wires connecting it to the PCB.

Fig. 2. (a) Measurement and simulation results of the photocurrent profiles when moving the x-axis direction to estimate the alignment tolerance by SMF. (b) Responsivity of the 10 elements.

layer thickness [16]. To minimize capacitance-related limitations while maintaining efficient carrier collection, we employed PIN junction structures with 50 μm diameters and 2.8 μm thickness. When the number of elements reaches the hundreds, it's difficult to do the impedance matching on the chip. The resistor footprint elevates manufacturing costs and packaging complexity. It is difficult to quantify and accurately control the gold wire length and the amount of silver epoxy. Therefore, we strive to maintain impedance matching as much as possible during PCB routing and connector interfacing. This work focuses on PCB level optimization of the high-speed electrical paths and impedance control, rather than changes to the PDA chip itself, yielding measurable receiver performance improvements.

In the PCB design, the impedance of traces is calculated using a layer stack manager with a field solver in Altium Designer [17]. To achieve a 50 Ω impedance and reduce reflections, along with the narrowest bond pads around the chip, the thinnest available dielectric between the top layer and ground layer was required. The dielectric thickness in our design is 75 μm, while the rest of the PCB structure serves as mechanical support to achieve a total thickness of 1.6 mm. The grounded coplanar waveguides (GCPWs) were used, where the signal lines and ground lines on both sides are located on the same metal layer, with a continuous ground plane on the bottom layer. Ten elements were selected for a fan-out design. They were located in the central part of the chip and were connected to the PCB via wire bonding and further connected to 10 coaxial connectors. The conductive silver epoxy was used to bond the chip to the PCB, with the PCB leaving a small hole (4.5 mm × 4.5 mm) to enable illumination. The transmission lines connecting the gold wires and RF connectors were optimized to an impedance of 50 Ω ($Z_0 = 50\,\Omega$). RF connectors were soldered to the PCB via 10 GCPWs transmission lines. The packaging enables high responsivity, with the generated photocurrents in each element being collected and output. When illuminating the entire PDA, all elements in the photosensitive area simultaneously will generate photocurrent. We fabricated and packaged a receiver module for optical measurements, DC characterization, eye diagram analysis, and bit error rate (BER) measurement. The packaged receiver module is shown in Fig. 1.
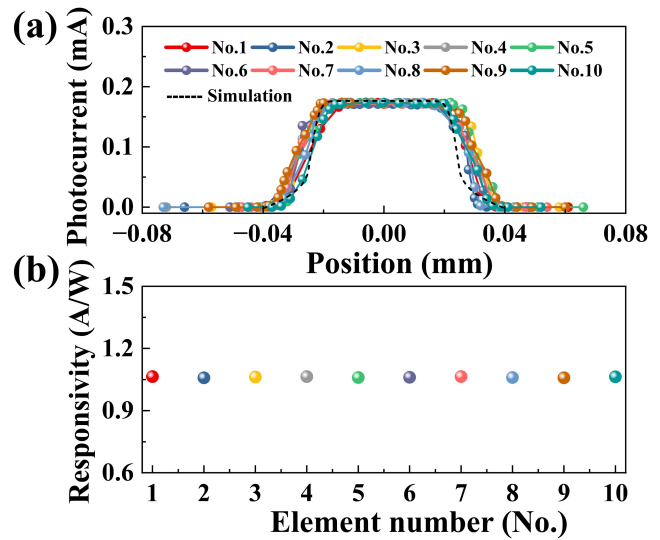
Characterization and results. To characterize the response of the elements in the receiver, photocurrent profiles at different positions were considered to assess alignment tolerance. We simulated the photocurrent to lateral displacement using a Gaussian aperture overlap model. The measurements of the receiver module were performed using an experimental setup consisting of a tunable laser (Santec TSL510), a power meter (Newport 1936-R), and a semiconductor parameter analyzer (Keithley 2400), which supplied reverse voltage and measured photocurrent when the receiver module was illuminated. Incident light was delivered through a single-mode fiber (SMF) with a Gaussian waist diameter of 10.4 μm.

The fiber positions were monitored with a Thorlabs camera and controlled using a micro stage (1 μm resolution) and a goniometer (Thorlabs GNL10/M) at 0° incidence, while the fiber was positioned close to the element surface to reduce laser profile effects. The alignment tolerance measurements were conducted on 10 elements along the x-axis of the array, revealing that the average position range for maintaining maximum photocurrent in an element was $\Delta x = 37\,\mu m$, as shown in Fig. 2(a). The measurement results closely matched the simulation. Within the optimal range, fiber light was fully absorbed and photocurrent declined outside this zone, though some light was still detected in insensitive areas. Although position differences between different elements were observed due to mechanical setup errors, all measurement results for beam size and position demonstrated great potential for PDA reception, suggesting high optical alignment robustness compared to the SMF field alignment tolerance of 10 μm.

The responsivity was performed under 5 V reverse bias voltage, measuring 10 elements at 1550 nm wavelength while ensuring maximum photocurrent at room temperature (23°C). All 10 elements demonstrated a responsivity over 1.0 A/W with excellent uniformity across the array, as shown in Fig. 2(b). The PDA responsivity was determined by measuring current-power (I-P) curves, where output photocurrent was recorded at different incident optical powers and the slope calculated through linear fitting represented the device responsivity. The measure-

ment conditions were kept constant to eliminate external factor influences. The PDA achieved high responsivity and enhanced tolerance to beam misalignment by enlarging the photosensitive area. It ensures that even when the incident light shifts during transmission, the elements in the PDA can still effectively capture optical signals, thereby demonstrating stability and robustness in practical applications.

The frequency response characteristics of the receiver module were measured using a Vector Network Analyzer (VNA, Rohde&Schwarz ZNB). Figure 3(a) compares the 3 dB, 6 dB, and 10 dB bandwidth of this work with prior work [18]. The average 3 dB bandwidth among the 10 elements increased from 2.0 GHz to 2.7 GHz, while the average 6 dB and 10 dB bandwidths increased from 2.9 to 4.8 GHz and 4.0 to 7.4 GHz, respectively. These bandwidth enhancements were attributed to the optimized track line design on the PCB. The inset of Fig. 3(a) shows the modulation response of the 10 elements. Practical large scale PDAs encounter design challenges in on-chip impedance matching, since thin-film resistors enlarge chip area and require isolation for high frequency consistency. Despite the presence of parasitic components causing fluctuations, we focus on the overall trend of the response curve rather than individual peaks. Figure 3(b) also shows the frequency response of element No.1 in the PDA under various reverse bias voltages with −5.5 dBm input optical power. At 1 V reverse bias voltage, the 3 dB bandwidth is measured 2.2 GHz, but increasing the reverse voltage to 5 V resulted in the bandwidth increasing to 2.8 GHz under identical optical power. The bandwidth increases with reverse bias, which shows that higher reverse bias effectively enhances the high frequency response.

The high data rate reception capabilities after long transmission distances of the receiver module were characterized. Both non-return-to-zero (NRZ) and 4-level pulse amplitude modulation (PAM-4) signals were measured. At the transmitter side, the optical signal generation system comprised the tunable laser and LiNbO$_3$ Mach–Zehnder intensity modulator (MZI) driven by an arbitrary waveform generator (AWG, Keysight M8195A) to produce both NRZ and PAM-4 data streams. An erbium-doped fiber amplifier (EDFA) and optical bandpass filter (OBPF) were used to amplify the optical power and control the wavelength transmission characteristics, while a 25 km SMF link was used for long-distance transmission. The optical signal emerged from a bare fiber end facet and was incident directly on the receiver under controlled conditions that simulated free-space coupling. The receiver was preceded by a variable optical attenuator (VOA) to precisely control the incident optical power.

Initially, the eye diagram was measured for each element at a data rate of 10 Gbps to establish performance, and the optical power was maintained at −5.5 dBm throughout the measurements. The RF signal was amplified by a linear broadband amplifier to enhance the peak-to-peak voltage at the input of the sampling oscilloscope (OSC, Keysight DCA-X 86100D). As the channel introduces distortion to the transmitted signal, an equalization process is required to decrease the impact. Equalization is achieved by applying the inverse of the channel response, thereby compensating for channel impairments. Among the various equalization techniques, one widely used approach is Zero Forcing (ZF), which is applied here at the transmitter side to optimize signal quality. The block diagrams of the transmitter (Tx) and receiver (Rx) module scheme are shown in Fig. 4(a).
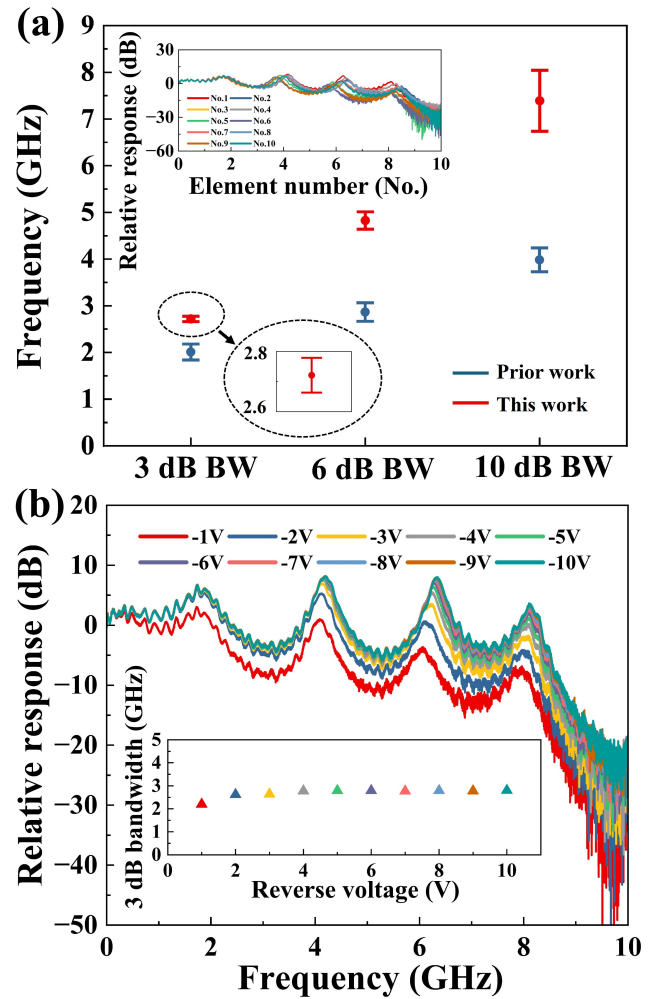

Fig. 3. (a) Comparison of the RF performance between prior work and this work. Inset: measured frequency responses under 5 V reverse bias voltage for 10 elements. BW: bandwidth. (b) Measured frequency responses and 3 dB bandwidth under different reverse voltages from −10 V to −1 V for element No. 1.

As shown in Fig. 4(b), the equalized performance of all 10 elements was consistent, each exhibiting clear eye diagrams up to 10 Gbps with large openings. The measured 10 Gbps eye diagrams for all elements under the same input power and similar output photocurrent were almost identical. The amplitude of the eye is an average of 96 mV at −0.3 mA.

The quality of the transmission link was also estimated through BER measurements using the same experimental setup. Due to a limited memory of the oscilloscope, very low BER values (below 10^{-5}) could not be measured using error counting. These very low BER values were derived from the Q-factor that was listed by the OSC. Higher BER values were obtained by error counting, i.e., the data obtained after the receiver were compared to the data generated at the transmitter side. The BER for element No.1 in the receiver module across varying bit rates from 8 Gbps to 20 Gbps, as presented in Fig. 5(a), confirms a large eye opening up to 7.5 GHz/15 Gbps for on-off keying (OOK) data transmission with NRZ format. The eye diagrams for PAM-4 signals are given in the same figure for different bit rates (10 Gbps and 16 Gbps). The BER measurements for NRZ
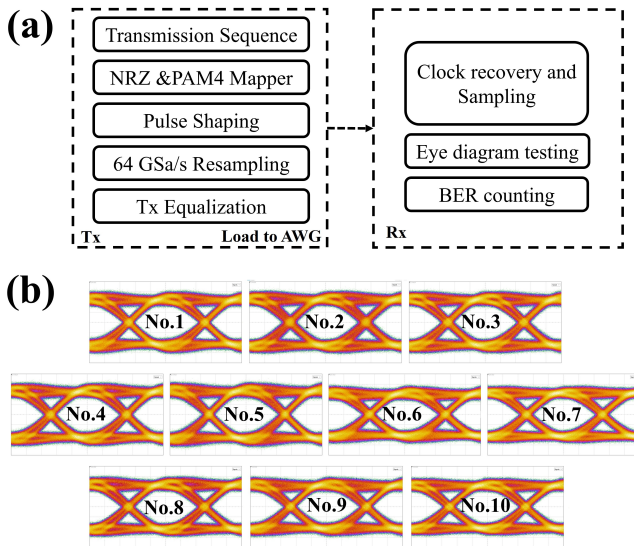
(a)

(b)

Fig. 4. (a) Block diagrams of the Tx and the Rx scheme. (b) Measured 10 Gbps NRZ eye diagrams for the 10 elements.

were extended to all 10 elements. As shown in Fig. 5(b), BER values below 1×10^{-12} were achieved under -4.5 dBm optical power for all elements, with minimal variation in received power requirements. The consistent achievement of clear eyes confirms the uniformity and high-speed reliability of the receiver module.

Conclusion. We have proposed and demonstrated a compact, high-performance receiver module using a 10-element PDA for robust O/E conversion. The integrated receiver module with 2.7 GHz average bandwidth demonstrated high responsivity (1.0 A/W), large optical alignment tolerance (37 μm) and high-frequency RF transmission capability. In a proof of concept demonstration for long-distance transmission, we successfully achieved the transmission of 10 Gbps NRZ signals over a hybrid 25 km optical fiber link under static conditions with BER below 10^{-12} and validated the system capability for high data rate communication. This work paves the way for high-speed RoFSO systems, bridging optical and wireless networks for future spatially multiplexed interconnects in datacom and 5G/6G applications.

Disclosures. The authors declare no conflicts of interest.

Data availability. Data underlying the results presented in this paper are not publicly available at this time but may be obtained from the authors upon reasonable request.
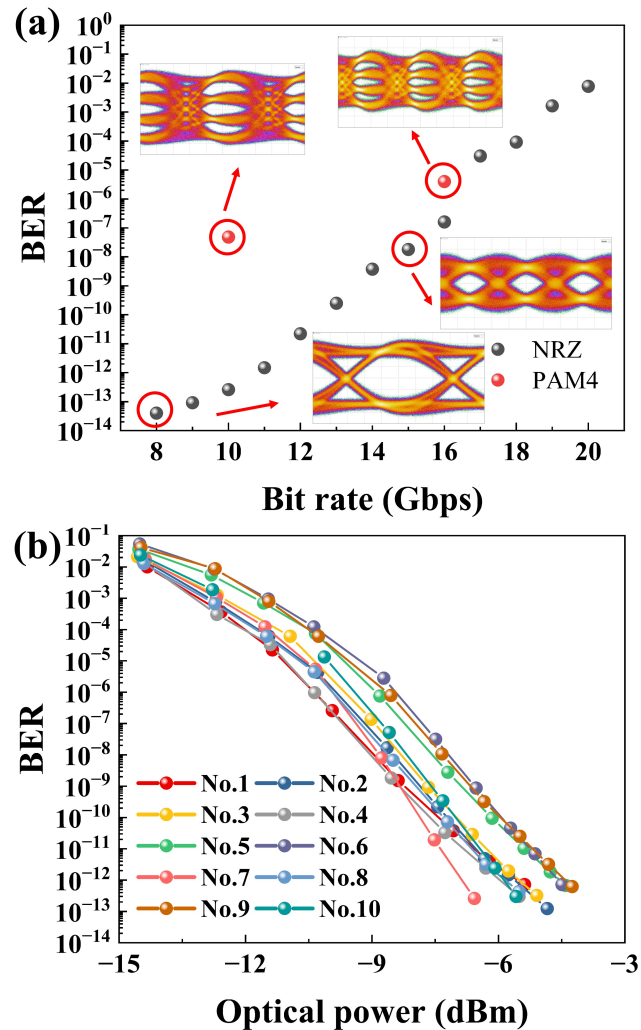
(a)

(b)

Fig. 5. (a) BER of NRZ and PAM-4 signals at various bit rates, measured for element No.1. (b) The BER measurement results were performed on 10 elements at 10 Gbps NRZ.

REFERENCES

1. H. Huawei, "5g wireless network planning solution white paper," Tech. Rep. (Huawei, 2018).
2. F. Liu, Y. Cui, C. Masouros, *et al.*, IEEE J. Sel. Areas Commun. **40**, 1728 (2022).
3. C.-X. Wang, X. You, X. Gao, *et al.*, IEEE Commun. Surv. Tutor. **25**, 905 (2023).
4. J. Yao, J. Light. Technol. **40**, 6595 (2022).
5. W. Niu, Z. Xu, Y. Liu, *et al.*, J. Light. Technol. **41**, 3316 (2023).
6. Y. Lei, X. Yan, C. Li, *et al.*, Opt. Lett. **47**, 2578 (2022).
7. Z. Zeng, S. Fu, H. Zhang, *et al.*, IEEE Commun. Surv. Tutor. **19**, 204 (2017).
8. H. Haas, L. Yin, C. Chen, *et al.*, J. Opt. Commun. Netw. **12**, A190 (2019).
9. T. Umezawa, Y. Yoshida, A. Kanno, *et al.*, J. Light. Technol. **39**, 1040 (2020).
10. Y. Hong, F. Feng, K. R. Bottrill, *et al.*, Opt. Express **29**, 33694 (2021).
11. H.-H. Lu, X.-H. Huang, W.-S. Tsai, *et al.*, Opt. Lett. **46**, 1269 (2021).
12. T. Umezawa, P. T. Dat, K. Jitsuno, *et al.*, J. Light. Technol. **39**, 5270 (2021).
13. X. Yang, W. Yuan, X. Duan, *et al.*, IEEE J. Quantum Electron. **60**, 1 (2024).
14. A. Gomez, K. Shi, C. Quintana, *et al.*, J. Light. Technol. **34**, 2510 (2016).
15. T. Matsui, Y. Sagae, Y. Yamada, *et al.*, J. Light. Technol. **42**, 4124 (2024).
16. Y. Xu and Q. Lin, Appl. Phys. Rev. **7**, 011315 (2020).
17. Altium, "Altium Designer," 2025, https://www.altium.com/altium-designer.
18. Y. Yan, M. Yang, S. Han, *et al.*, Opt. Lett. **50**, 2526 (2025).